XVI International Conference on Computational Plasticity. Fundamentals and Applications
COMPLAS 2021
E. Oñate, D. Peric, M. Chiumenti and Eduardo de Souza Neto (Eds)

NEW RESULTS IN 3D-MESOMECHANICAL COUPLED ANALYSIS OF EXTERNAL SULPHATE ATTACK IN CONCRETE

C. BISCARO[*], A. MARTINEZ[†], A. PÉREZ[†], C.M. LÓPEZ[†], G. XOTTA[1] AND I. CAROL[†]

[*] Department of Civil, Environmental and Architectural Engineering
Università degli Studi di Padova
Via Marzolo, 9 – 35131 Padova, Italia
e-mail: caterina.biscaro@phd.unipd.it, giovanna.xotta@unipd.it, www.unipd.it/en/icea

[†] Department of Civil and Environmental Engineering
Universidad Politècnica de Cataluña
Jordi Girona 1, Edif D2, E-08034 Barcelona, Spain
e-mail: ariadna.martinez.e@upc.edu, adria.perez@upc.edu, carlos.maria.lopez@upc.edu, ignacio.carol@upc.edu

Key words: External Sulphate Attack, concrete degradation, chemo-mechanical modeling, interface element

Summary. External Sulphate Attack (ESA) is one of the main degradation processes affecting concrete structures. It takes place when the concrete is in an environment rich in sulphate ions and with a high humidity index. Once it has penetrated the concrete, sulphate undergoes chemical reactions that lead to the precipitation of expansive ettringite crystals that cause volumetric expansions of the cement paste/mortar, eventually leading to cracking and damage. The FE analysis is undertaken by representing concrete as composed by aggregate pieces inserted in a cement/mortar matrix. Zero-thickness interface elements are pre-inserted to represent potential fractures along all aggregate-matrix as well as along some selected matrix-matrix element contacts. An existing fracture-based non-linear constitutive law is used for the interface elements. Concerning the reactive transport problem, the model follows previous work in the same research group, which combined an older approach from the literature for the continuum medium, with interface elements in the context of meso-mechanical analysis of concrete specimens in 2D, as well as initial work in 3D (but no coupling). In the present paper, the effects of the coupling between mechanical and diffusion/reaction in 3D are introduced and demonstrated. The new results obtained confirm that, also in 3D, penetration of ions, expansive reactions as well as subsequent cracking and degradation, all take place much faster when the coupling effect due to the open interfaces is introduced.

1 INTRODUCTION

In recent years there has been an increasing interest in the study of the modelling capacity of concrete deterioration processes due to the combined effects of mechanical and environmental actions, i.e. concerning the mechanics of durability. Among other types of chemical attack, external sulphate attack (ESA) is one of the most significant degradation processes that affect the durability of concrete.

Sulphate attack in concrete is generally caused by sulphate ions moving into the concrete from the surrounding environment; the reactions lead to the formation of additional ettringite, process also known as "secondary ettringite formation", which occupies more volume than the reaction products and therefore is an expansive reaction with potentially deteriorating effects [1-3]. ESA can lead to cracking, spalling and eventually, under severe and sustained attack conditions, to the complete disintegration of the material [4,6].

The aim of this study is to extend and update previous work in the group of Mechanics of Materials UPC on the meso-mechanical analysis of ESA using the FEM with zero-thickness interface elements. Previous work departed from a numerical representation of the diffusion-reaction sulphate attack process for the continuum medium proposed by Tixier and Mobasher [7], which was combined with a meso-mechanical representation for concrete based on the FEM with interface elements [8,9]. Integration those two models, with the addition of a localized diffusivity along open cracks which strongly depends on crack opening, led to the 2D model of Idiart et al [10], that still to date, seems to be the only one considering C-M coupling via discrete cracks (see for instance [11] for a recent review of the existing numerical models for ESA), and that is capable of representing neatly physical effects such as "onion-peeling" degradation observed in experiments. The model extension to 3D was initiated in [12] but with no C-M coupling effects. In the present paper, the effects of the coupling between mechanical and diffusion/reaction in 3D are introduced and demonstrated.

2 MESOMECHANICAL MODEL

In the meso-mechanical model used in this study, concrete is represented as a composite material, where large aggregates are embedded in a porous matrix. A continuum type-model is adopted for both components, which from the mechanical viewpoint are considered linear elastic. The possibilities of failure are provided by zero-thickness interface elements equipped with a fracture-based constitutive law, that are inserted along the contact surfaces between the aggregates and the matrix and along potential fracture planes within the matrix itself. The interface constitutive model was originally proposed for 2D analysis in [13] and then improved and expanded for 3D analysis [8,14].

The interface behavior is formulated in terms of the normal and shear components of the stresses on the interface plane $\boldsymbol{\sigma} = [\sigma_N, \tau_1, \tau_2]^t$ and the corresponding relative displacements $\boldsymbol{u} = [u_N, u_1, u_2]^t$ (t = transposed), which may be identified as crack opening/sliding. The loading (plasticity) function is defined as a three-parameter hyperbola:

$$F(\boldsymbol{\sigma}) = -(c - \sigma_N \tan\phi) + \sqrt{\tau^2 + (c - \chi tan\phi)^2} \quad (1)$$

where τ is the modulus of the shear stresses ($\tau = \sqrt{\tau_1^2 + \tau_2^2}$), χ is the tensile strength and corresponds to the normal stress at vertex of the hyperbola, c is the apparent cohesion and $\tan\phi$ is the internal friction angle. The last two parameters define the asymptote to the hyperbola, as shown in Figure 1.

As the stress state reaches the surface $F(\sigma_N, \tau) = 0$ and cracking starts, the loading surface begins to shrink due to the decrease in the main parameters according to evolution laws based on the work dissipated in fracture process (W^{cr}). The increment of the work dissipated is calculated as the increment of plastic work, from which the shear frictional work is subtracted in compression.

Two limit fracture situations may occur. The classical tensile ("Mode I") fracture mode is reached in the presence of pure tensile tress. A second limit situation corresponds to fracture along a plane subject to shear and very high compression ("Mode IIa"). The hyperbolic fracture surface provides a smooth transition between these two limit loading situations. To control these fracture modes, the model has two parameters representing the Mode I fracture energy G_f^I (pure tension), and the "asymptotic Mode II" (or Mode IIa) fracture energy G_f^{IIa} (shear/compression).

The model is associated in tension ($Q = F$), but not in compression, where dilatancy vanishes progressively for $\sigma_N \to \sigma_{dil}$ dil (Figure 1). Dilatancy is also decreased as the fracture process progresses, so that it vanishes for $W^{cr} = G_f^{IIa}$.

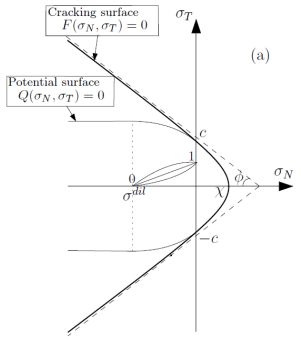

Figure 1: Hyperbolic fracture surface F and plastic potential Q [8]

3 CHEMICAL TRANSPORT MODEL

The diffusion-reaction problem is formulated on the basis of the simplified approach proposed by Tixier and Mobasher [7], which was later modified by Idiart et al. [10]. External sulphate attack is assumed to depend on the concentration of only one diffusing species, the sulphate ions, which is the main variable of the reactive transport model.

Sulphate entering the concrete first reacts with portlandite (CH) to form gypsum. Once the gypsum is formed it can react with the four different phases of calcium aluminate ($C_4AH_{13}, C_4A\bar{S}H_{12}, C_3A$ and C_4AF) leading to the formation of secondary ettringite ($C_6A\bar{S}_3H_{32}$). These reactions can be grouped as follows:

$$C + q\bar{S} \to C_6A\bar{S}_3H_{32} \tag{2}$$

where C is the equivalent molar concentration of the grouped reaction of calcium aluminate and q is the stoichiometric coefficient weighted for each reaction.

These quantities can be determined by a second-order diffusion-reaction equation for sulphate concentration and an additional equation for the evolution of calcium aluminates:

$$\frac{\partial U}{\partial t} = \frac{\partial}{\partial t}\left(D_U \frac{\partial U}{\partial x}\right) - kUC; \qquad \frac{\partial C}{\partial t} = -k\frac{UC}{q} \qquad on\ \Omega \tag{3}$$

where: U (mol/m^3) is the sulphate concentration, D_U (m^2/s) is the sulfate ion diffusion coefficient through the porous medium, C (mol/m^3) is the quantity of calcium aluminate equivalent, k (m^3/mol s) is the grouped sulfate reaction rate and x is the space coordinate.

Sulphate ion diffusion can occur within the cement matrix and along the fracture lines. In the matrix, this process depends on the porosity of the material: initially, the greater the diffusion if the greater its porosity; in a second step, the diffusivity will decrease as the pores become progressively filled with the material product of the chemical reaction [10]. In this case, D_U is expressed by the following hyperbolic function:

$$D_U(\phi_{cap}) = D_0 + (D_1 - D_0) f(\beta_D, \phi_{cap}) \tag{4}$$

where D_1 and D_0 are the maximum and minimum diffusion values, ϕ_{cap} is the actualized capillary porosity that is reduced with the formation of ettringite, $f(\beta_D, \phi_{cap})$ is the scale function that depends on a shape factor (β_D) expressing the non-linearity of the D_U variation and on the ratio between the actualized and the initial capillarity.

Diffusivity along the fracture lines, represented in the FE mesh by zero-thickness interface elements, depends on fracture opening and it may increase for the lines that become open cracks, as the sulphate attack progresses and diffusivity in the pores of the bulk decreases. The diffusivity value is defined by a power function of the crack aperture [10].

According to the following formulas, the volumetric strain of the solid material is expected to be proportional to the amount of reacted calcium aluminate:

$$\varepsilon_v(t) = \alpha_s \cdot CA_{react} - f \cdot \Phi_{ini} \tag{5}$$

where CA_{react} is the molar concentration of equivalent calcium aluminates that have reacted, which can be calculated as the difference between the initial concentration CA_0 and the residual unreacted concentration at a given time, C:

$$CA_{react} = CA_0 - C \tag{6}$$

In (5), Φ_{ini} denotes the initial porosity, and f denotes the percentage of the initial porosity that must be filled with precipitates before any material expansion may occur, with typical values ranging from 0.05 and 0.40 [7]. Finally, α_s is the average solid material volumetric expansion per unit molar concentration of reacted aluminates, which can be written as:

$$\alpha_s = m^{ettr} - m^{CA} - q \cdot m^{gypsum} \tag{7}$$

where m^{ettr}, m^{CA} and m^{gypsum} are the averaged molar volumes of ettringite, aluminates and gypsum [m^3/mol], respectively.

The mechanical model and the diffusion-reaction model are implemented through two computational programs that are coupled with each other *via* a "staggered" scheme. The Finite Element codes, developed by the MECMAT-UPC group, are respectively DRAC, for the mechanical problem, and DRACFLOW, for the diffusion-reaction problem. The results are represented through the use of the post-processor GID. The mechanical code DRAC has MPI parallel processing capabilities which was essential to run 3D cases in reasonable times.

4 APPLICATION EXAMPLE

The 3D geometry considered for the application example is represented in Figure 5. It corresponds to a prismatic specimen of 40x40x60mm which represents ¼ of a column section subject to sulphate attack from the external surface (two of the six specimen faces). The specimen geometry consists of 42 aggregate pieces embedded in a mortar matrix, which is

discretized using 18518 tetrahedral continuum elements, 26698 triangular interface elements, with a total of 51795 nodes.

For the boundary conditions of the mechanical problem, displacements are restricted in the normal direction of the four faces in contact with the rest of the column, leaving the other two vertical faces free. For the diffusion problem, convective boundary conditions (mixed Newmann-Dirichlet with imposed flux $q_n = K_{conv} * (c - c_{sol})$ are imposed on the two external vertical faces with a (maximum) solution sodium sulphate concentration of $c_{sol} = 35.2$ mol/m^3 and convective constant $K_{conv} = 0.1$ m/day, while free boundary (zero flow) is applied on the remaining four faces.

The parameter values of the chemical-reaction problem are: $D_1 = 1.70 * 10^{-3}$ cm^2/day, $k = 2 * 10^{-5}$ (m^3/(mol·day)), $q = 3$, $f = 0.05$, $w/c = 0.5$, $\alpha = 0.9$, $D_0/D_1 = 5 * 10^{-2}$, $\beta_D = 1.5$, $\alpha_S = 2.98 * 10^{-4}$, $[C_3A]_{inicial} = 200$ (mol/m^3). For the mechanical analysis, the aggregate and the mortar are considered linear elastic with parameters: $E = 70000$ MPa (aggregates), $E = 25000$ MPa (mortar) and $\nu = 0.20$ (both). For the aggregate-mortar interfaces the parameters are: $K_N = K_T = 100000$ MPa/mm, $\tan\phi_0 = 0.70$, $\tan\phi_{res} = 0.40$, $\chi_0 = 2$ MPa, $c_0 = 7$ MPa, $G_F^I = 0.03$ Nmm, $G_F^{II} = 0.3$ Nmm. For the mortar-mortar interfaces the same parameters are used with the exception of $\chi_0 = 4$ MPa, $c_0 = 14$ MPa and $G_F^I = 0.06$ Nmm (and therefore, $G_F^{II} = 0.6$ Nmm).

The analysis is run twice, first considering uncoupled analysis (constant diffusivity of interfaces) and then as a coupled analysis (considering variable interface diffusivity increasing with crack opening). In the uncoupled analysis the results of the mechanical problem do not enter and do not influence the solution of the chemical problem, while in the coupled case the model evaluates deformations of the mechanical problem which then alter the diffusion/reaction calculation leading to an iterative problem that (as explained in previous section) is solved using a staggered strategy.

In Fig. 2, the progress of sulphate, ettringite, porosity and diffusivity observed from the upper face of the specimen, are shown at three specific times for both the uncoupled analysis and for the coupled analysis. Looking at the sulphate progress in the two cases it can be observed that, while in the uncoupled analysis the sulfate concentration remains fairly stable, in the coupled one the sulphate concentration fronts progressively penetrate deeper in the specimen.

The ettringite fronts also move towards the interior of the sample, with a delay with respect to the sulphate concentration front because of the (non-infinite) reaction rate. In both cases, uncoupled and coupled, the increase in ettringite formation leads to a reduction in porosity and diffusivity from the exposed edges towards the inside of the sample. The main difference between the two cases is due to the fracture generated by the expansion process and to the higher overall sulphate diffusivity in the coupled case due to the high transmissivity of the open joints, which causes a greater and progressive penetration of the sulphate front. In the uncoupled case, on the other hand, the large reduction in diffusivity results in a "plugging" effect which strongly limits the possibility of sulphate entering from the outside thus causing a much more limited penetration of the sulphate within the sample, basically limited to a thin layer near the specimen boundary.

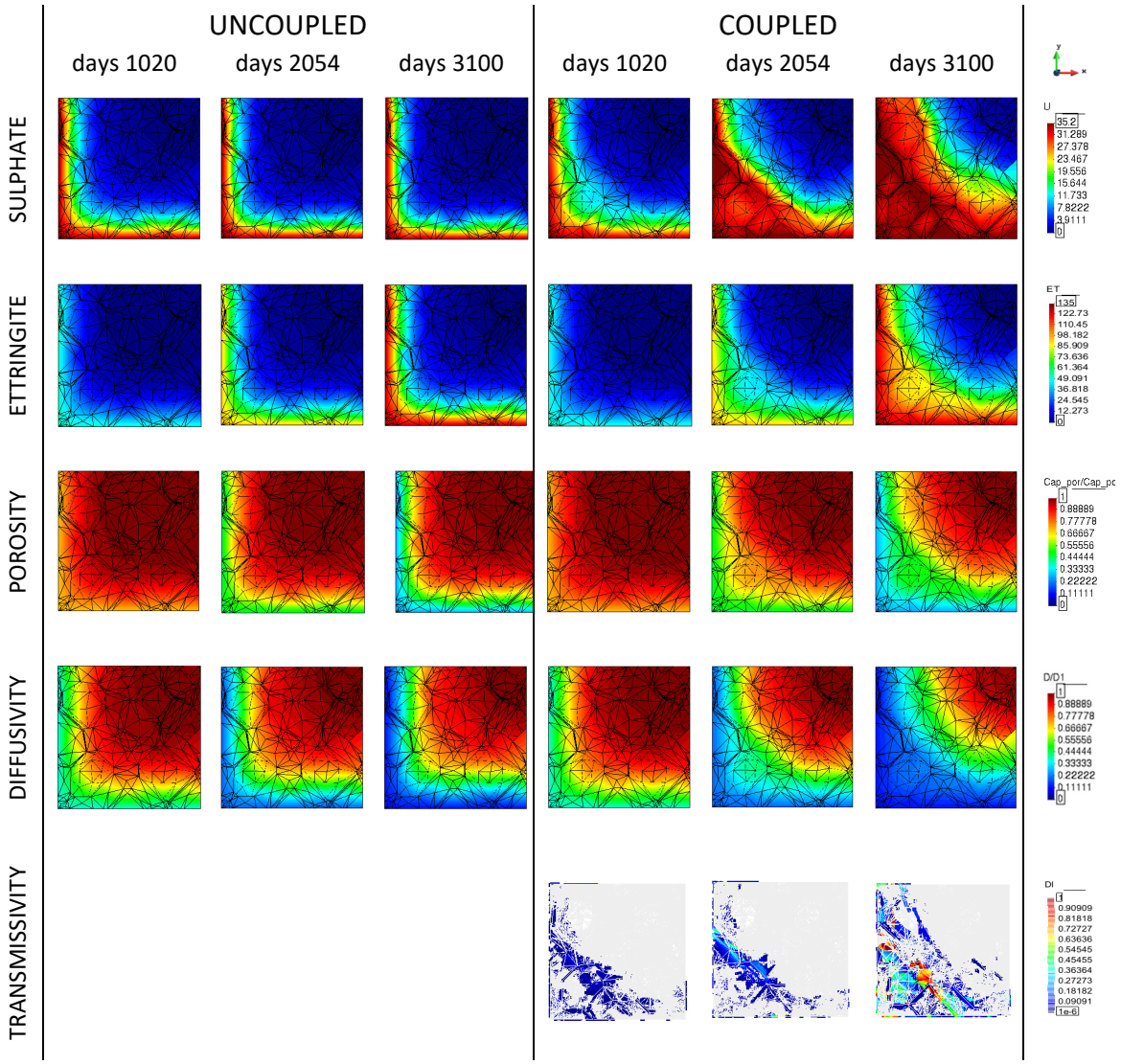

Figure 2: Results of the uncoupled and coupled analysis: contour plots on the upper face of specimen, of sulphate [mol/m^3], ettringite [kg/m^3], porosity, diffusivity and transmissivity [cm^3/day], all at three different times (t = 1020, 2054 and 3100 days).

Finally, three-dimensional representations for the two cases at a final time of 3100 days are shown to highlight the differences between the two cases. In Figure 3 the aggregates have not been represented (space left as voids) in order to visualize better the penetration fronts, and to make clearer the significant difference between the uncoupled and coupled cases.

Figure 4 illustrates a comparison of the displacement intensities at 3100 days; the level of degradation in the coupled case is much higher than in the uncoupled one, although the failure mode seems very similar in both cases.

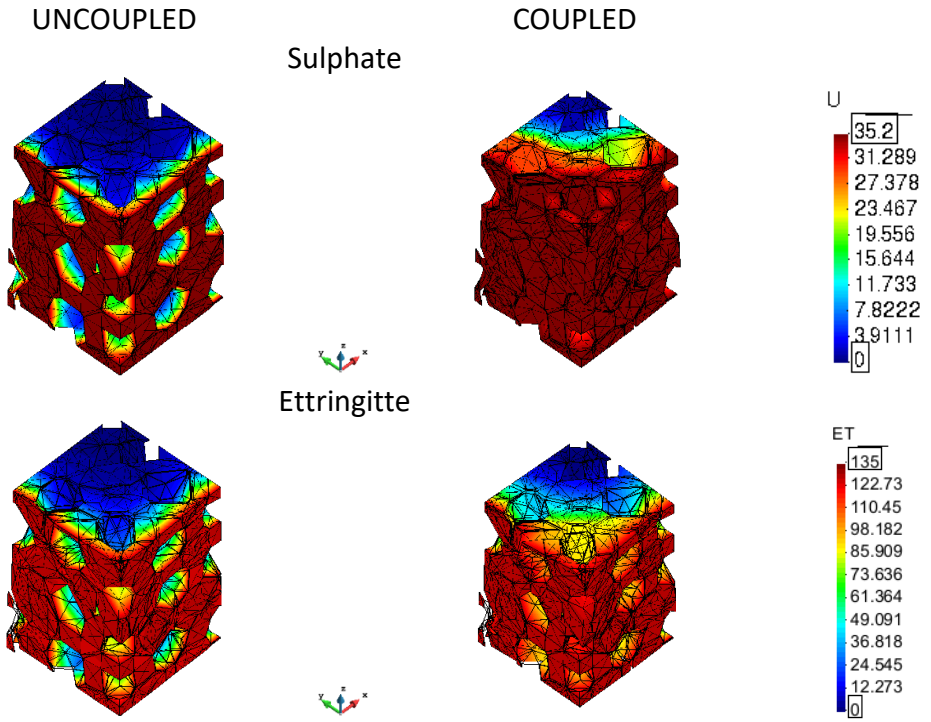

Figure 3: Side view of the specimen at 3100 days; comparison between uncoupled and coupled cases for sulphate and ettringite distributions.

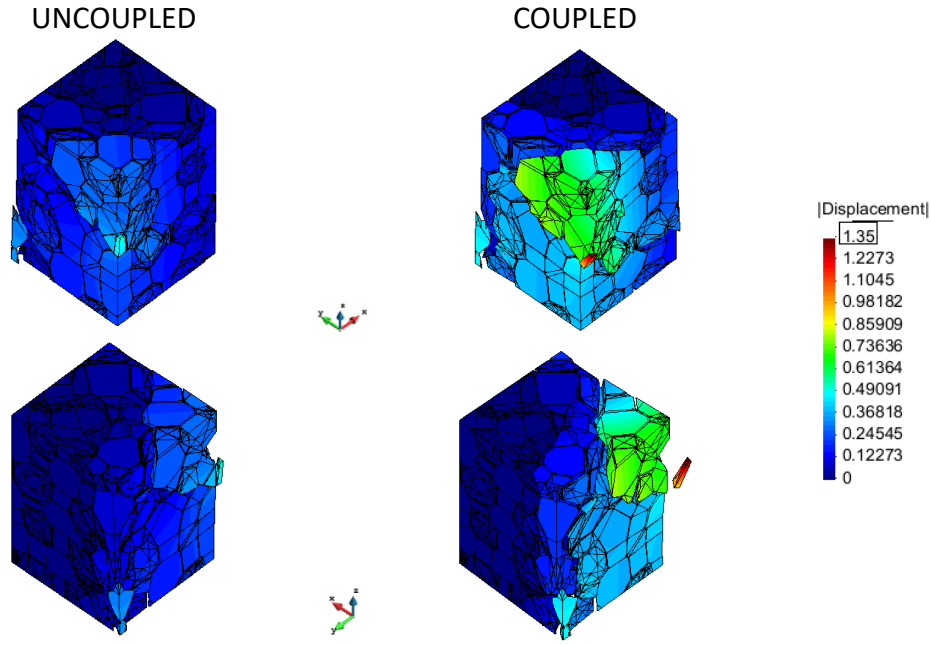

Figure 4: Comparison of displacement intensity fields, between uncoupled and coupled case at 3100 days.

In Figure 5, which shows the deformed mesh at 3100 days with the aggregates in black and the porous matrix in grey, it can be observed that in both cases there is a vertical crack that opens from the top to the bottom of the specimen. The analysis has required, both in the uncoupled and coupled cases, the elimination of elements and nodes from some pieces of material which became totally detached from the rest of specimen due to fully developed fractures.

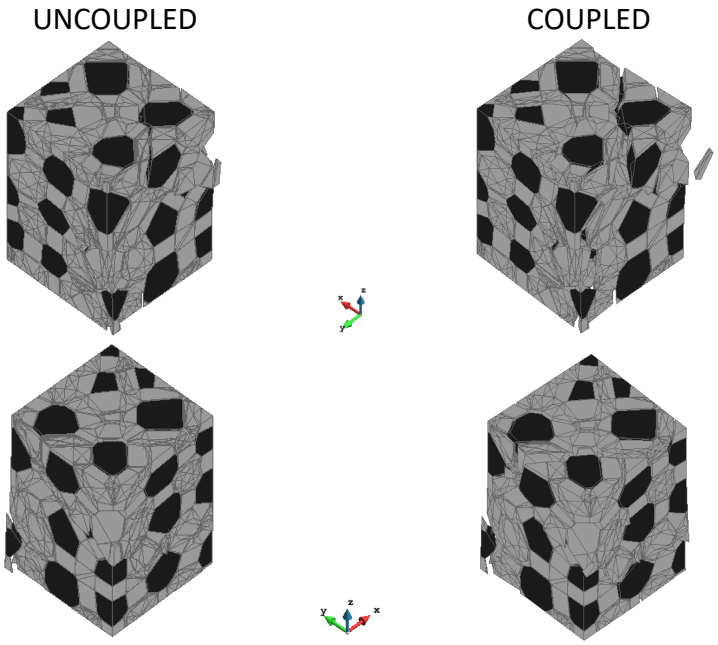

Figure 5: Comparison of two side views of deformed mesh at 3100 days, between uncoupled and coupled cases. In black the aggregates, in grey the porous matrix.

5 CONCLUDING REMARKS

The model used in this work is a powerful tool, able to represent the complex three-dimensional degradation behaviour of concrete under the action of External Sulphate Attack (ESA).

The results of the coupled analysis clearly show the effect of cracking on the diffusion process. Since the cracking is connected to the edges of the sample, this modelling enhances the influence of fractures as preferential pathways of sulphate penetration; thus, leading to an increase in ettringite production and subsequent volume expansions, and consequently to a greater internal cracking with an acceleration of the deterioration process of the sample. In the coupled case, the level of degradation is much higher than in the uncoupled case, although the mode of failure is similar in both cases. Therefore, the results obtained confirm that the coupled simulation is more realistic than the uncoupled one to represent the behaviour of concrete samples subjected to the action of a severe external sulphate attack, as the results agree better with experimental observations.

It can also be noted that, again in both cases, in the corner formed by the two faces in contact with the sulphate, the concentration of volumetric deformations gives rise to the formation of fractures which are located on inclined planes with respect to the exposed external faces and

which develop vertically along the sample, leaving some material pieces totally disconnected from the rest of the specimen. These pieces are removed in the calculation using the "excavation" feature of the code. The removal of these pieces corresponds in fact to the physical phenomenon of spalling, that is a well-documented phenomenon occurring in this type of chemical attack and, as shown, can be captured naturally in the type of analysis proposed.

ACKNOWLEDGMENTS

This research is supported by grants BIA2016-76543-R from MEC (Madrid), which includes FEDER funds, and 2017SGR-1153 from AGAUR (Generalitat de Catalunya, Barcelona).

REFERENCES

[1] Brown, P. and Hooton, H. Ettringite and thaumasite formation in laboratory concretes prepared using sul-fate-resisting cements. *Cem. Concr. Comp.*, **24**:361-70 (2002).

[2] Al-Amoudi, O. Attack on plain and blended cements exposed to aggressive sulfate environments. *Cem. Concr. Comp.* (2002) **24**:305-316.

[3] Irassar, E., Bonavetti, V. and González, M. Micro-structural study of sulfate attack on ordinary and limestone Portland cements at ambient temperature. *Cem. Concr. Res.* (2003) **33**:31-41.

[4] Lee, S., Hooton, R., Jung, H., Park, D. and Choi, C. Effect of limestone filler on the deterioration of mortars and pastes exposed to sulfate solutions at ambient temperature. *Cem. Concr. Res.* (2008) **38**:68-76.

[5] Santhanam, M., Cohen, M.D. and Olek, J. Mechanism of sulfate attack: a fresh look. Part 1: Summary of experimental results. *Cem. Concr. Res.* (2002) **32**:325-332.

[6] Schmidt, T., Lothenbach, B., Romer, M., Neuenschwander, J. and Scrivener, K. Physical and microstructural aspects of sulfate attack on ordinary and limestone blended Portland cements. *Cem. Concr. Res.* (2009) **39**:1111-1121.

[7] Tixier, R. and Mobasher, B. Modeling of damage in cement-based materials subjected to external sulphate attack. I: Formulation. II: Comparison with experiments. *ASCE J. Mat. Civil Engng.* (2003) **15**:305-322.

[8] Carol, I., Lopez, C.M. and Roa, O. Micromechanical analysis of quasi-brittle materials using fracture-based interface elements. *International Journal for Numerical Methods in Engineering*. (2001) **52**:193-215.

[9] Caballero, A., Carol, I. and López, C.M. A meso-level approach to the 3D numerical analysis of crackimg and fracture of concrete materials. *Fatigue and Fracture of Engineering Materials and Structures* (2006) **20**:979-991.

[10] Idiart, A., López, C.M. and Carol, I. Chemo-mechanical analysis of concrete cracking and degradetion due to sulphate attack: a meso-scale model. *Cem. Concr. Compos*. (2011) **33:**411-423.

[11] Ikumi, T.; Segura, I. Numerical assessment of external sulfate attack in concrete structures. A review. *Cem. Concr. Res.* (2019) 121:91-105.

[12] Pérez, A., Riera, C., López, C.M. and Carol, I. 3D-Mesomechanical analysis of the external sulfate attack in concrete. *Proceedings of the XIV International Conference on Computational Plasticity: Fundamentals and Applications*, (5-7September Barcelona, Spain) (2017) p:276-287

[13] Carol, I., Prat, P.C. and López, C.M. Normal/shear cracking model: application to discrete crack analysis. *Journal of Engineering Mechanics* (1997) **123**:765-773.

[14] Caballero, A., Willam, K., and Carol, I. Consistent tangent formulation for 3D interface modeling of cracking/fracture in quasi-brittle materials. *Comp. Meth. Appl. Mech. Engrg*. (2008) **197**:2804–2822.